Population of high-L sulfur Rydberg levels by ion–Rydberg-atom charge exchange

F. J. Deck, E. A. Hessels,* and S. R. Lundeen
Department of Physics, University of Notre Dame, Notre Dame, Indiana 46556
(Received 14 July 1993)

A fast beam of sulfur Rydberg atoms is formed by charge exchange from an 11-keV beam of S^+ ions in a crossed thermal rubidium beam, laser-excited to the $10F$ or $8F$ levels. Population of specific $n=9,10$ sulfur Rydberg levels is studied by selective excitation with a Doppler-tuned CO_2 laser followed by field ionization. Complete spectral resolution of levels with $L \geq 4$ allows a direct study of the populations in specific nL levels and reveals distinctly nonstatistical distributions of population in L. The results are compared with predictions of a classical Monte Carlo three-body collision theory, revealing some similarities, but also clear differences.

PACS number(s): 34.70.+e, 42.62.Fi

Ion–Rydberg-atom charge exchange from positive ion beams in a Rydberg-atom target is an attractive method of forming a wide variety of fast Rydberg beams since it offers the possibility of controlling the binding energy of the fast Rydberg atoms through choice of the excitation energy of the charge-exchange target. Theoretical studies of the ion–Rydberg-atom charge-exchange process [1],

$$X^+ + Y(n_T) \longrightarrow X(n) + Y^+ ,$$

suggest, for example, that if $n_T = 10$ and the ion velocity is close to the matching velocity $v = 1/10$ a.u., more than 50% of the charge-transfer products will be formed in levels with $8 \leq n \leq 12$. The resulting high concentration of fast Rydberg population in levels with $n \cong n_T$ could lead to substantial improvements in studies already carried out with fast Rydberg beams [2–4], and also make possible new types of studies in which such selective population is a critical feature.

Understanding of the ion–Rydberg-atom charge-transfer process has been advanced through the experiments of MacAdam [5], who studied production of $18 < n < 54$ states in ion collisions with laser-excited Na atoms, using field-ionization detection. The most complete theoretical treatment of the process has been obtained with classical Monte Carlo methods [1], which account for many features of the existing experiments. The predictions most critical to applications in the production of Rydberg beams are the n and L distributions of Rydberg-level populations produced under specific collision conditions. While the n distributions have been studied in previous experiments [5], there have been no previous studies of the predicted strongly nonstatistical L distributions found in the Monte Carlo calculations of the ion–Rydberg-atom charge-transfer process [1]. This is in contrast to studies of the related process of charge transfer from atomic ground states by highly-charged ions, where recent experiments which distinguish different L levels by their different optical decay paths and lifetimes have provided some confirmation of the L distributions predicted by similar Monte Carlo calculations [6]. The study reported here provides a more direct test of the rather different L distributions predicted for the ion–Rydberg-atom charge-transfer process. While some features of our observations are similar to theoretical predictions, the details of the L distributions are rather poorly predicted by theory.

Figure 1 illustrates the apparatus used for this study. A S^+-ion beam is produced in a duoplasmatron ion source, accelerated to an energy of 11 keV ($v = 0.12$ a.u.), and magnetically analyzed. After passing through an optional gas-charge-exchange cell (normally empty), the S^+ beam intersects the laser-excited Rb beam where it is partially neutralized to form the fast sulfur beam. Atoms formed in specific $n = 9, 10$ levels are selectively detected by excitation with a Doppler-tuned CO_2 laser; either 9-17 or 10-30 transitions can be conveniently excited at appropriate Doppler tuning angles, either with the $R(18)$ or $R(20)$ lines in the 10.4-μm band of the CO_2 laser. In either case, immediately after excitation the upper state of the transition is Stark ionized and the resulting ions deflected into a channeltron detector. A weak deflection field after the laser deflects residual S^+ ions out of the beam. Sulfur atoms formed in the Rb target travel in a nominally-field-free region until reaching the excitation laser, encountering only stray electric fields, estimated to be ≤ 0.5 V/cm.

The vertical Rb beam is formed in a 700-K oven whose exit nozzle is 1.4 cm below the S^+ beam axis. Three cw lasers, propagating in a horizontal plane and intersecting at small angles, excite the Rb beam at its points of intersection with the S^+ beam. The lasers provide stepwise excitation of ^{85}Rb from the $F = 3$ ground state to either the $8F$ or $10F$ state via the sequence of transitions:

(1) $5\,^2S_{1/2}(F=3)$ to $5\,^2P_{3/2}(F=4)$, $\lambda = 780$ nm, $\tau_P = 27$ nsec.

(2) $5\,^2P_{3/2}(F=4)$ to $4\,^2D_{5/2}(F=5)$, $\lambda = 1529$ nm, $\tau_D = 86$ nsec.

(3) (a) $5\,^2D_{5/2}(F=5)$ to $8\,^2F_{7/2}(F=6)$, $\lambda = 792$ nm, $\tau_{8F} \cong 350$ nsec or (b) $5\,^2D_{5/2}(F=5)$ to $10\,^2F_{7/2}(F=6)$, $\lambda = 755$ nm, $\tau_{10F} \cong 700$ nsec.

*Permanent address: Department of Physics, York University, North York, Ontario, Canada M3J 1P3.

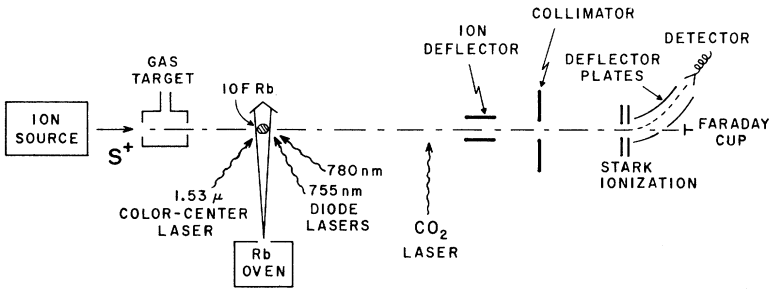

FIG. 1. Schematic diagram showing apparatus used to study formation of sulfur Rydberg states in charge-transfer collisions with laser-excited Rb atoms. An 11-KeV S^+-ion beam crosses a thermal Rb beam excited by three cw lasers to the $10F$ (or $8F$) state. Sulfur atoms formed in $n=9$ or 10 levels with $L \geq 4$ are selectively detected by resonant excitation with a Doppler-tuned CO_2 laser to a more weakly bound level, which is then Stark ionized, and the resulting ions collected.

The first two of these transitions are "cycling transitions" in which the spontaneous decay of the upper level can only repopulate the lower level. The third transition is not, since decays to other $nD_{5/2}(F=5)$ states occur in about 50% of the decays, but all such decays quickly repopulate the $F=3$ ground state and therefore do not lead to net-population loss from the four-level system. The third transition does not resolve the hyperfine structure of the $nF_{7/2}$ level, but relies on the spin-matrix elements to favor the indicated transition over the transition to the $F=5$ hyperfine level by a factor of about 10. The relatively rare transitions to this level are also not expected to lead to substantial population loss from the four-level system during the dwell time ($\cong 2$ μsec) of the rubidium atoms in the laser beams.

The Rb target volume is about 8 mm^3, and the density of $8F$ (or $10F$) levels is estimated from the power absorbed on the third laser transition to be about 10^9 cm^{-3}. This is about 5% of the initial $5\,^2S_{1/2}(F=3)$ population, as estimated from the absorption at the first laser transition. The presence of the F-state population is quite apparent even to the naked eye by the blue visible emission produced in cascade decays through the $6\,^2P_{3/2}$ level.

The 755, 780, and 792 lasers are low-power diode lasers (Sharp LT030, LT022, and Panasonic LN9705, respectively), with spectral bandwidths of approximately 50 MHz and output powers of about 3 mW. The 1529-nm laser is a color-center laser (Burleigh FCL-120), with a spectral bandwidth of ≤ 10 MHz and an output power of about 10 mW. All three lasers are linearly polarized in the vertical direction. The frequencies of the three excitation lasers are controlled in a slow feedback loop which tunes the first and third lasers to the centers of their respective absorption lines, and the second laser to achieve maximum fluorescence at 1.5 μm. With occasional manual adjustment, this produces stable operation of the Rydberg target over many hours.

Typical S^+-beam intensity is $\cong 50$ nA, as measured with the Faraday cup at the end of the beam. The Faraday cup was operated as a neutral beam detector by biasing it at -22.5 V to enhance secondary emission. Under these conditions, its yield was calibrated as $\cong 3.3(3)$ secondary electrons per neutral atom. The fractional neutralization measured with the Rydberg target was small ($f \cong 10^{-3}$), consistent with the target thickness implied by the calculated total charge-exchange cross section of 2×10^{-12} cm^2 [1]. Despite this, the $n=9,10$ populations, measured with the CO_2 laser, were considerably greater with the Rydberg target than with the gas cell. In a typical case, e.g., the $10H$ level, the ratio of CO_2 signal to neutral beam was 10^4 times larger with the Rydberg target, and the CO_2 signal itself was 50 times larger with the Rydberg target than with the gas cell. In addition, the ratio of CO_2 laser signal to background ion flux, which is present due to Stark ionization of atoms formed initially in ionizable high-n levels, was three times larger with the Rydberg target than with the gas cell. Both of these observations are consistent with the expected high concentration of neutral sulfur population in levels with $n \cong n_T$.

Figure 2 illustrates the detection of high-L $n=10$ sulfur populations, using the CO_2 laser. It shows the CO_2-induced ion flux, after 10-30 excitations, as a function of the Doppler-tuning angle. The vertical scale has been calibrated by estimating the gain of the channeltron, through measurements of shot noise in the amplified ion current. Because of the large dipole polarizability of S^+, the $n=10$ fine structure is completely resolved up to the highest value of L ($L=9$). To a good approximation, the binding energies of the Rydberg levels excited by the laser are given by

$$E(n,L) = -R/n^2 - (\tfrac{1}{2})e^2\alpha_d\langle r^{-4}\rangle_{nL} , \qquad (1)$$

where $R=1$ Ry. The solid vertical bars show the fitted positions of $10L$-$30(L+1)$ transitions, adjusting the di-

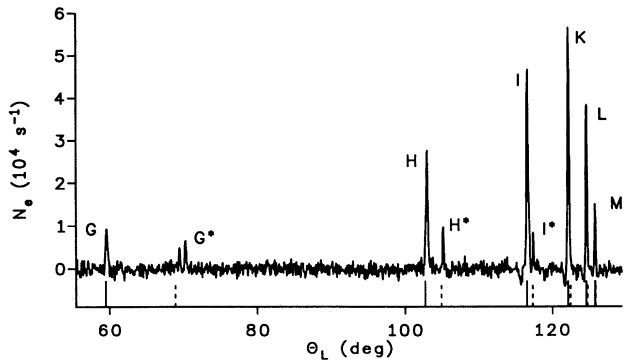

FIG. 2. Ion flux observed as a function of Doppler-tuning angle of the CO_2 laser, $\nu_L = 975.9304$ cm^{-1}, showing the excitation of $n=10$, $4 \leq L \leq 9$ levels to $n=30$. The peaks, labeled by the initial L represent transitions to an $n=30$ level with $L=L+1$, except in the cases marked with asterisks, which are transitions to states with $L=L-1$. The solid and dashed vertical bars show the fitted line positions in each case, according to Eq. (1), with $\alpha_d = 10.6a_0^3$.

pole polarizability (α_d) and the zero offset of the Doppler-tuning angle. While such a simple model is not expected to be completely successful, since it accounts neither for higher-order effects in the sulfur fine structure nor for possible sinusoidal errors in the Doppler-tuning angle [7], it is quite adequate to identify the transitions unambiguously. Also apparent in the data of Fig. 2 are weaker transitions corresponding to the transitions $10L$-$30(L-1)$ for the cases $L=4,5,6$. The calculated positions of these lines (in the same model) are shown as dashed vertical bars. The vertical height of each signal, when compared with the total neutral beam intensity, can be used to deduce the fractional population of each of the $n=10$ levels studied. In a very similar manner, the populations of the $n=9$ levels with $L=5,6,7,8$ can be studied from the resolved fine structure of the 9–17 CO_2 excitations. The Stark ionizer could be adjusted to detect either $n=30$ levels or $n=17$ levels. A slightly different field configuration was used in each case. To detect $n=30$, a transverse electric field of about 1500 V/cm was used, while to detect $n=17$, a longitudinal field of about 9000 V/cm was used.

In order to measure the population distributions produced in the $n=9$ and 10 levels of sulfur by each Rydberg target ($8F$ or $10F$), each $\Delta L=+1$ excitation peak in the two spectra was carefully scanned, measuring simultaneously the ion current produced by the CO_2 laser and the neutral beam current due to the Rydberg target. The ratio of ion current to beam current was plotted as a function of Doppler-tuning angle and fit to extract the linewidth and the ratio of ion current to beam current at line center. The fitted linewidths varied from 0.32° to 0.55°, according to the strength of the dipole matrix elements for each transition. This indicates that the strongest transitions are well saturated and power broadened. The weaker transitions are expected to be excited somewhat less efficiently, as is shown, for instance, by the reduced strengths of the $\Delta L=-1$ transitions compared with the $\Delta L=+1$ transitions. The variation of excitation efficiency with transition strength was modeled as the excitation of an inhomogeneously broadened beam population characterized by an angular width of 0.12° by a power broadened homogeneous excitation function. Calculated transition matrix elements and resulting excitation efficiencies for each transition studied are shown in Table I.

The measured ratios between ion current and beam current at the centers of each of the excitation lines are closely related to the ratio of the population of a particularly sulfur Rydberg level (N_{nL}) to the total population (N_T). Specifically, we assume that

$$I_b=\epsilon e N_T \ , \tag{2}$$

$$I_e=N_{nL}e^{-t/\tau}T(nL)Cge \ , \tag{3}$$

where I_b is the measured secondary-emission current on the Faraday cup and I_e is the Stark ionization current at the output of the channeltron when the laser is tuned to excite the nL level. In Eq. (2), ϵ is the secondary electron yield, measured to be 3.3(3), and e is the electron charge. In Eq. (3), g is the gain of the channeltron, C is the ionization-collection efficiency of the Stark ionizer [estimated to be 0.7(2)], $T(nL)$ is the calculated excitation efficiency from Table I, τ is the radiative lifetime of the nL Rydberg level [8], and t is the 2.77-μsec transit time from the Rydberg target to the CO_2 laser interaction region. The channeltron gain g was estimated to be 1000 for the $n=10$ signals, and 1800 for the $n=9$ signals, the difference being attributed to the higher kinetic energy of the ions produced in the longitudinal stripping field. Neglected in Eq. (3) is the transfer of population into the nL level as a result of spontaneous decay from higher levels (cascades) or stimulated transitions (blackbody radiation) from nearby levels. Modeling of these effects, using the detailed population distributions predicted by theory, indicates that they are insufficient to substantially alter our conclusions. Using Eqs. (2) and (3), N_{nL}/N_T can be computed from the measured ratios I_e/I_b. The results are shown, for both $8F$ and $10F$ Rydberg targets, in Table II. The error bars shown there correspond to the statistical errors in the measured ratios only, as determined by repeated measurements, and do not include uncertainties in the factors discussed above which contribute a common uncertainty of about 30% to all the results. Also shown in Table II are predicted values of $\sigma(nL)/\sigma_T$, the ratio of charge-exchange cross section into a particular level to the total-calculated total-capture cross section, as computed by Olson in a classical three-body model of the near-resonant capture process, using Monte Carlo methods [9].

The population fractions measured with the $8F$ target show a very clear nonstatistical L distribution, as illustrated in Fig. 3(a). The solid points show the experimentally determined population fractions. For comparison, a statistical distribution normalized for best fit to the measured fractions is shown by a dashed line. In both the $n=9$ and 10 levels, the population fraction shows a maximum at about $L=6$ and then decreases at the highest L values. This behavior is remarkably similar to the predictions of the classical Monte Carlo calculations, illustrated as open circles in Fig. 3. Since the plotted error bars in the experimental numbers do not include the common

TABLE I. Matrix elements and calculated excitation efficiencies for several Rydberg-atom–Rydberg-atom transitions.

Transition	$z_{\rm rms}(a_0)$	$T(n,L)$
$9H$-$17I$	1.191	0.490
$9I$-$17K$	1.040	0.475
$9K$-$17L$	0.786	0.437
$9L$-$17M$	0.448	0.360
$10G$-$30H$	0.447	0.355
$10G$-$30F$	0.088	0.115
$10H$-$30I$	0.423	0.337
$10H$-$30G$	0.062	0.075
$10I$-$30K$	0.371	0.332
$10I$-$30H$	0.040	0.060
$10K$-$30L$	0.292	0.305
$10L$-$30M$	0.193	0.245
$10M$-$30N$	0.094	0.150

TABLE II. Measured ratios of peak Stark ionization to secondary electron currents (I_e/I_b) for each $\Delta L=+1$ laser signal, and the deduced fractional population of several Rydberg states of sulfur from near-resonant charge exchange with the $8F$ and $10F$ rubidium targets at $v=0.12$ a.u. The last column gives the predictions of a classical Monte Carlo calculation [9].

Level	I_e/I_b	$N(nL)/N_T$	$\sigma(nL)/\sigma_T$
	Rb($8F$) Target		
$9H$	25.0(44)	0.0472(83)	0.0277(14)
$9I$	43.2(64)	0.0473(70)	0.0341(15)
$9K$	50.2(86)	0.0419(72)	0.0327(15)
$9L$	42.0(64)	0.0334(51)	0.0167(11)
$10G$	19.0(42)	0.0228(50)	0.0223(12)
$10H$	44.6(62)	0.0334(46)	0.0296(14)
$10I$	73.2(128)	0.0416(73)	0.0331(15)
$10K$	76.6(132)	0.0394(68)	0.0368(16)
$10L$	59.4(102)	0.0338(58)	0.0218(12)
$10M$	22.8(40)	0.0195(34)	0.0056(6)
	Rb($10F$) Target		
$9H$	13.3(8)	0.0250(14)	0.0112(10)
$9I$	28.4(16)	0.0311(18)	0.0128(10)
$9K$	36.6(58)	0.0305(48)	0.0128(10)
$9L$	41.8(32)	0.0332(25)	0.0087(9)
$10G$	12.4(8)	0.0149(10)	0.0123(10)
$10H$	48.0(22)	0.0360(17)	0.0134(10)
$10I$	89.8(50)	0.0510(28)	0.0121(10)
$10K$	100.0(60)	0.0515(31)	0.0131(10)
$10L$	86.0(96)	0.0489(55)	0.0101(10)
$10M$	37.4(48)	0.0319(41)	0.0081(9)

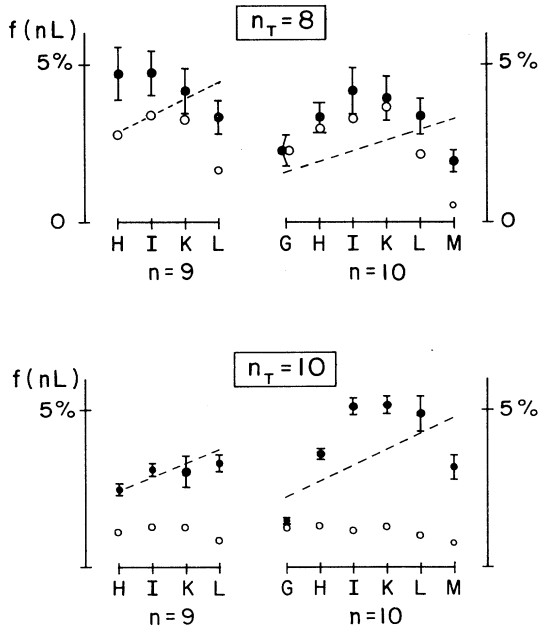

FIG. 3. Fractional population of several $n=9,10$ Rydberg levels, as measured (solid points) and as calculated [9] using classical Monte Carlo methods (open points). The dashed lines show a population distribution proportional to the statistical weights $(2L+1)$, normalized for a best fit of the measurements. The theoretical points have statistical errors comparable to the size of the plotted points.

30% uncertainty, the agreement with theory appears to be nearly perfect.

Unfortunately, the populations observed with the $10F$ target are in much poorer agreement with theory, as illustrated in Fig. 3(b). The $n=9$ population fractions in this case are close to statistical, as shown by the dashed-line fit. This is in contrast with the theoretical predictions of a flat, or slightly falling distribution in L. The $n=10$ population fractions look very different, with a pronounced peaking of the population around $L=7$, but again not at all like the predictions of theory. Not only are the measured L distributions qualitatively different from theoretical predictions, in the case of the $10F$ target, but the size of the population fractions is consistently larger than theory as well. This indicates a tighter concentration of population near $n\cong n_T$ than is predicted by theory.

The L distributions produced by the $8F$ and $10F$ targets are much more similar than theory predicts. Nevertheless, there are real, though subtle, differences between the two cases, which can be demonstrated by taking the ratio between the measured population fractions for the $8F$ and $10F$ targets. The ratio is insensitive to uncertainties in common overall factors such as secondary electron yield or channeltron gain, and also insensitive to errors in L-dependent factors such as excitation efficiency. The measured ratios plotted in Fig. 4 show a monotonic decrease with L in both $n=9$ and 10 levels, indicating that the L distributions produced by the two targets are indeed significantly different. The $8F$ target is systematically less effective than the $10F$ in producing high-L states. This trend is reminiscent of the general theoretical prediction that the production of very high-L states is reduced when $n\geq n_T$ [1]. However, as shown in Fig. 4, the deficiency predicted by theory is confined to the very highest-L states ($L=8,9$), in contrast to the monotonic trend seen throughout the measurements. So while there are some points of agreement between the observed and predicted L distributions, the overall agreement is certainly not good. Without reference to theoretical predictions, the measurements show clearly that the Rydberg levels can be populated in highly nonstatistical patterns in ion–Rydberg-atom charge exchange, and that these patterns can be quite sensitive to the principal quantum number of the Rydberg target.

Another aspect of the Rydberg-level populations produced in near-resonant charge exchange is the distribu-

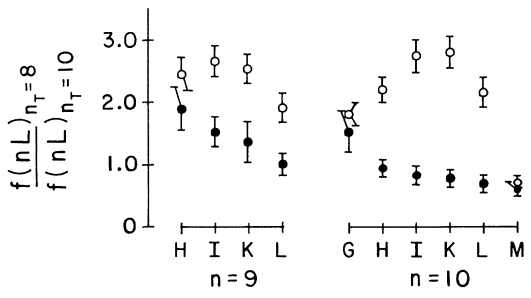

FIG. 4. Ratios of fractional populations (Fig. 3) obtained with $8F$ and $10F$ targets for $n=9,10$ Rydberg levels.

tion of level populations in n. For example, which Rydberg target, $8F$ or $10F$, is more efficient in producing, say, $10I$ population? Naively, one might expect the $10F$ target to produce a larger fraction of its population in such an $n=10$ level (since $n=n_T$), and therefore expect the ratio plotted in Fig. 4 to be less than 1. This indeed proves to be the case for some of the $n=10$ levels studied, e.g., the $10I$, but not for others. Apparently, the distribution of population in n is not independent of L. For example, the $8F$ target is more efficient than the $10F$ target in producing $10G$ states, while the reverse is true for producing $10I$ states. The calculation incorrectly predicts greater efficiency for the $8F$ target in all cases but one ($10M$). It would be possible to do a much more complete study of the n distributions by using a more widely tunable laser for the third excitation step of the Rydberg target. Unfortunately, it would be much more difficult to extend beyond $n=9,10$ the range of levels whose populations are monitored with the CO_2 laser.

This study establishes that Rydberg levels populated in ion–Rydberg-atom charge exchange near the matching velocity show sharply nonstatistical population distributions in L. In the case of $n=9$ and 10 levels, the L distributions are found to be significantly different for $8F$ and $10F$ Rydberg targets, demonstrating a sensitive dependence on the principal quantum number of the Rydberg target. Although some features of the observed L distributions are similar to theoretical predictions, there are also very clear discrepancies. The fragmentary information obtained relating to n distributions also suggests some significant differences with the theory. The aspect of the ion–Rydberg-atom charge-transfer process that is most important for applications in forming Rydberg beams is the degree of concentration of the populations in n levels near that of the target. The measurements reported here show a high degree of population concentration, in some cases even higher than predicted by theory, and certainly sufficient to confirm the attractiveness of this application. The strong L dependence revealed by this study can be used to good advantage in such applications. It could, for instance, greatly simplify studies of L-changing collision processes by providing control over the initial L distributions of the Rydberg beam.

In a broader context, this study confirms what had already been suggested by the existing theoretical calculations, that the phenomenology of ion–Rydberg-atom charge transfer is rich in detail. However, it appears that it may be premature to rely on calculations to predict these details. In applications to natural systems, for example, the formation of high-L Rydberg emission lines in the solar atmosphere [10], many of these details could be crucial to understanding the role of ion–Rydberg-atom charge exchange. For example, the measurements of Fig. 3(b) show population inversions on several $10\rightarrow 9$ transitions that are not predicted by the theory.

This work was supported by the National Science Foundation under Grant No. PHY90-19064. John R. Brandenberger and John F. Plumb assisted in the early phases of the experiment. We thank Ron Olson for providing results of unpublished calculations.

[1] J. Pascale, R. E. Olson, and C. O. Reinhold, Phys. Rev. A **42**, 5305 (1990).

[2] E. A. Hessels, P. W. Arcuni, F. J. Deck, and S. R. Lundeen, Phys. Rev. A **46**, 2622 (1992).

[3] Z. W. Fu, E. A. Hessels, and S. R. Lundeen, Phys. Rev. A **46**, R5313 (1992).

[4] Peter M. Koch, in *Rydberg States of Atoms and Molecules,* edited by R. F. Stebbings and F. B. Dunning (Cambridge University Press, Cambridge, 1983), p. 473.

[5] K. B. MacAdam, in *Atomic Physics 12,* edited by Jens C. Zorn and Robert R. Lewis, AIP Conf. Proc. No. 233 (A.I.P., New York, 1991), p. 310; K. B. MacAdam, L. G. Gray, and R. G. Rolfes, Phys. Rev. A **42**, 5269 (1990).

[6] E. Wolfrum, R. Hoekstra, F. J. de Heers, R. Morgenstern, and H. Winter, J. Phys. B **25**, 2597 (1992).

[7] W. G. Sturrus, E. A. Hessels, P. W. Arcuni, and S. R. Lundeen, Phys. Rev. A **38**, 135 (1988).

[8] Hydrogenic radiative lifetimes used were $\tau_{9H}=2.00$, $\tau_{9I}=2.77$, $\tau_{9K}=3.80$, $\tau_{9L}=4.91$, $\tau_{10G}=1.81$, $\tau_{10H}=2.75$, $\tau_{10I}=3.88$, $\tau_{10K}=5.21$, $\tau_{10L}=6.73$, $\tau_{10M}=8.43$. All in μsec.

[9] R. E. Olson (private communication), based on method of Ref. [1].

[10] E. S. Chang, E. H. Avrett, P. J. Mauas, R. W. Noyes, and R. Loeser, Astrophys. J. **379**, L79 (1991).